THE JOURNAL OF PHYSICAL CHEMISTRY C
A JOURNAL OF THE AMERICAN CHEMICAL SOCIETY

pubs.acs.org/JPCC

Article

Fused-Ring Carbon Nanothread Synthesized by Pressure-Induced Polymerization of Azulene

Xin Yang, Guangwei Che, Fang Li, Xingyu Tang, Yajie Wang, Yida Wang, Aijiao Guan, Junfeng Xiang, Qian Li, Jie Liu, Xiao Dong, Ho-kwang Mao, Haiyan Zheng,* and Kuo Li*

Cite This: J. Phys. Chem. C 2024, 128, 16011−16019

Read Online

ACCESS | Metrics & More | Article Recommendations | Supporting Information

ABSTRACT: sp^3-Carbon nanothreads (sp^3-CNTh) have attracted broad attention due to their one-dimensional diamond-based structure and predicted excellent mechanical and electrical properties. The quality of CNTh is significantly affected by defects and disorders, and the synthesis of ordered CNTh is still very challenging. Here, we successfully synthesized an orderly stacked fused-ring CNTh from azulene, with an obvious color change from blue to orange. At 1.2 GPa, azulene underwent a phase transition, as identified by in situ spectroscopy and X-ray diffraction (XRD). Above 15 GPa, azulene reacted irreversibly, forming an orderly stacked CNTh, confirmed by XRD and transmission electron microscopy. Solid-state nuclear magnetic resonance of CNTh revealed the presence of both sp^2- and sp^3-C. Our study reported an orderly stacked fused-ring CNTh and elucidated its formation through a high-pressure chemical reaction of azulene, which gives new insights into the pressure-induced polymerization of aromatics and is of benefit for designing and synthesizing new CNThs.

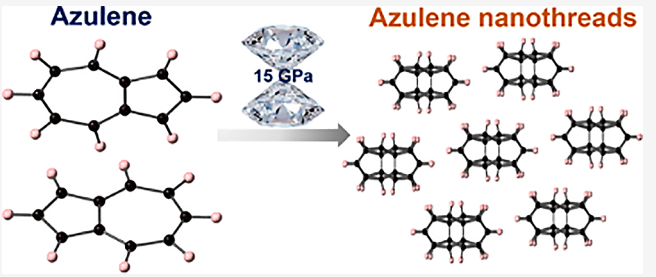

INTRODUCTION

The sp^3-carbon nanothread (sp^3-CNTh) is a one-dimensional (1D) sp^3 hydrocarbon, which was first identified in the pressure-induced polymerization product of benzene in 2015.[1] It was predicted to possess excellent strength and toughness,[2−4] as well as large band gap and high thermal conductivity,[5−7] making it a promising candidate for applications in sensors,[8] nanoelectromechanical systems, and energy storage devices.[2,9] However, benzene is herringbone-stacked at high pressure and the similar reactivity of its six carbon atoms leads to competing reaction pathways and complex product structures,[10−12] limiting the investigation of its novel properties and exploration of its application. Recently, several crystalline CNThs have been synthesized successively, including furan,[13,14] 2,5-furandicarboxylic acid,[15,16] aniline, etc.,[17] which employed heteroatoms to enhance selectivity and emphasized the importance of intermolecular interactions on molecular stacking, reaction processes, and crystalline products.

Electrostatic interaction is an important tool for modulating intermolecular stacking in crystal engineering. For example, in the benzene-hexafluorobenzene cocrystal, the strong electron-withdrawing effect of fluorine atoms in hexafluorobenzene results in opposite multipole (quadrupole moments) compared to benzene, which attracts them to each other along the normal of their planes and results in a face-to-face columnar stacking.[18] This intermolecular interaction is widely used in biological and chemical fields such as molecular recognition and self-assembly.[19,20] Similarly, 1:1 naphthalene/octafluoronaphthalene[21,22] and anthracene/octafluoronaphthalene[22] cocrystals maintain parallel displaced $\pi\cdots\pi$ stacking instead of the T-shaped interactions under high pressure, transforming into an ordered CNTh product. This strategy provides a novel and competitive approach to regulating molecular stacking and product structure under high pressure.

Azulene ($C_{10}H_8$) is an aromatic tautomer of naphthalene, consisting of a seven- and five-membered ring. This unique molecular structure has many different properties in terms of color, molecular orbital structure, and reaction selectivity, making it valuable for constructing organic functional materials with special optical activity.[23,24] More importantly, the electron-rich five-membered ring and electron-deficient seven-membered ring create a large dipole moment (1.08 D) between the two rings (Figure 1a).[25] This makes it promising to form an antiparallel stacking, where the five-membered ring is close to the seven-membered ring of its neighbor (Figure 1b)[26] and is expected to polymerize toward an ordered CNTh product under high pressure without introducing heteroatoms.

Received: July 8, 2024
Revised: September 2, 2024
Accepted: September 4, 2024
Published: September 17, 2024

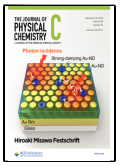

https://doi.org/10.1021/acs.jpcc.4c04557
J. Phys. Chem. C 2024, 128, 16011−16019

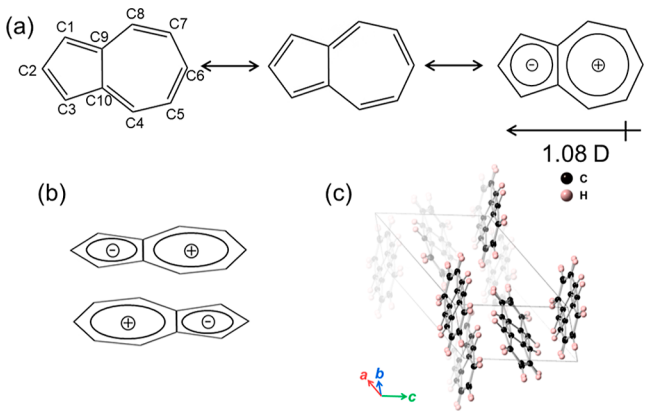

Figure 1. Structure of azulene. (a) Azulene and its polarized resonance structure with the dipole moment. (b) Antiparallel configuration of azulene dimers. (c) Disordered crystal structure of azulene at ambient conditions, with a 50% atomic occupancy.

In this study, we investigated the structure evolution and chemical reaction of azulene under high pressure using in situ Raman, infrared (IR), and UV−vis absorption spectroscopy and X-ray diffraction (XRD), as well as ex situ transmission electron microscopy (TEM), pair distribution function (PDF), and solid-state nuclear magnetic resonance (ssNMR). We found that azulene experienced a phase transition at ∼1.2 GPa, started polymerization at 15 GPa, and produced a fused-ring CNTh with excellent interthread order, likely related to intermolecular electrostatic interactions. Our study demonstrates that azulene, a molecule of historical interest, can serve as an effective precursor for constructing CNTh materials and highlights the importance of introducing a large dipole moment as a strategy for designing and synthesizing ordered CNThs.

METHODS

Materials and Synthesis of PE-20 Using a Paris-Edinburgh Press. Azulene ($C_{10}H_8$, 99%) was purchased from Alfa Aesar and used without further purification. The purity and crystalline phase were checked by powder XRD with Rietveld refinement, as shown in Figure S1. The large-volume product (PE-20) was synthesized using a VX3 Paris-Edinburg (PE) press under 20 GPa, equipped with double-toroidal (4 mm in diameter) diamond anvils and nonencapsulated T301 stainless-steel gaskets. The pressure was estimated from the Edinburgh group calibration curve, with an oil pressure of 1600 bar corresponding to 20 GPa on the sample.[27] An automatic hydraulic oil syringe pump was used to drive the system at 10 mL/min below 100 bar, 8 bar/min from 100 to 400 bar, 6 bar/min from 400 to 800 bar, 4 bar/min from 800 to 1000 bar, 2 bar/min from 1000 to 1200 bar, 1 bar/min from 1200 to 1400 bar, and 0.5 bar/min from 1400 to 1600 bar. Then it was decompressed to ambient conditions at the same rates. The unreacted azulene was dissolved and removed by ethanol.

High-Pressure Experiments. A symmetric diamond anvil cell (DAC) with 400 μm culet-type Ia diamonds was used for Raman and XRD experiments. Type IIa diamonds were used for IR and ultraviolet−visible (UV−vis) spectroscopy experiments. T301 stainless-steel gaskets were preindented to a thickness of 40 μm, and holes with d = 200 μm were drilled in the center of the indentation to serve as the sample chamber. The pressure was determined by measuring ruby fluorescence.[28] No pressure-transmitting medium was used for in situ Raman, IR spectroscopy, and synchrotron XRD measurements. Silicone oil was used as the pressure-transmitting medium for in situ UV−vis spectroscopy.

Raman, IR, and UV−vis Spectroscopy. In situ Raman experiments were performed on a Renishaw Raman microscope with a 785 nm line of Nd/YAG laser as the excitation source. The system was calibrated by the signal of silicon. IR experiments were performed in transmission mode on a Bruker VERTEX 70v FTIR spectrometer equipped with a HYPERION 2000 microscope. A Globar source was used, and spectra were collected in the range of 600−4000 cm^{-1} with a resolution of 2 cm^{-1}. The absorption of the empty DAC collected in the same aperture region was used as the background. UV−vis absorption experiments and optical images were collected in a home-designed spectroscopy system in the microregion (built by Ideaoptics) with a xenon light source from 200 to 1700 nm.

XRD and TEM. The in situ synchrotron XRD patterns under high pressure were collected at the beamline 4W2 of the Beijing Synchrotron Radiation Facility. The incident X-ray beam was monochromatized to a wavelength of 0.6199 Å, and the instrument was calibrated by CeO_2. The data were reduced by Dioptas software.[29] Jana 2006 and TOPAS V6 software were used for Rietveld refinements.[30] In the refinements, the azulene molecule was restrained as a rigid body. Laboratory XRD data were recorded on a PANalytical Empyrean diffractometer with monochromated Cu K_α radiation (λ = 1.5418 Å). TEM and selected area electron diffraction (SAED) experiments were performed on a JEM-2000 microscope under an accelerating voltage of 80 kV.

^{13}C Solid-State Nuclear Magnetic Resonance. ssNMR experiments were performed on a Bruker Avance NEO 400 MHz NMR spectrometer. The sample was filled in 3.2 mm ZrO_2 rotors. The quantitative ^{13}C NMR spectrum was measured using multiCP at 14 kHz magic angle spinning (MAS). The contact time and recycling delay were 2500 μs and 3 s, respectively.[12,31] The cross-polarization (^{1}H−^{13}C) (CP) nonquaternary suppression (NQS) ^{13}C NMR spectrum was collected with the addition of a dipolar dephasing delay of 60 μs at a MAS frequency of 10 kHz. The contact time and recycling delay were 2500 μs and 3 s, respectively. The ^{13}C chemical shifts were referenced to the methylene carbon of adamantane at 38.48 ppm. The sample temperature during the NMR experiments was about 300 K, and spectra were analyzed by using TopSpin and MestReNova software. The sp^2- and sp^3-C contents in the sample were determined by peak integration of the MultiCP data using MestReNova software. Based on the NMR discussions, a CNTh model was constructed. Then the computation (optimization/shielding tensor) was performed on a model with five layers using Gaussian 09 at the M06-2X/6-31G(d)//mPW1PW91/6-31G(d) level of theory.[32,33]

Total X-ray Scattering. Synchrotron total X-ray scattering data were collected on PE-20 at the 11-ID-B beamline of the Advanced Photon Source at the Argonne National Laboratory. The powder sample (∼10 mg) was loaded into a polyimide capillary. The incident X-ray beam was monochromatized to a wavelength of 0.2115 Å, and the instrument was calibrated by CeO_2. Dioptas software was used to reduce the collected 2D data and subtract the background of an empty capillary.[29] The PDF $G(r)$ data was reduced by PDF getX3 software[34] with a Q_{max} of 24.6 $Å^{-1}$.

https://doi.org/10.1021/acs.jpcc.4c04557
J. Phys. Chem. C 2024, 128, 16011−16019

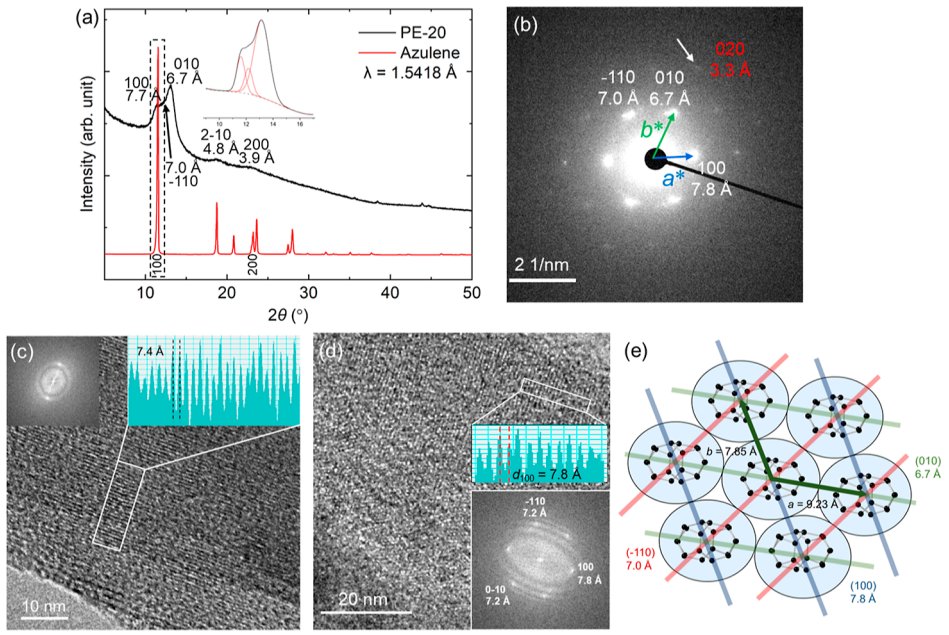

Figure 2. Crystallographic characterization of PE-20. (a) Lab XRD patterns of PE-20 and azulene. The inset displays the fitting result for the overlapping regions. (b) SAED pattern showing pseudohexagonal symmetry. (c) High-resolution transmission electron microscopy (HRTEM) image with the inset line profile and fast Fourier transform (FFT) pattern, revealing the 1-D structure. (d) HRTEM pattern of azulene DNTh viewed along the axis of the thread. The inset shows the FFT image. (e) Schematic plot for the proposed packings of azulene-CNTh, including a hypothetical intrathread structure to simulate the shape of the thread.

Density Functional Theory Calculations. Density functional theory (DFT) calculations were performed to investigate the reaction process of azulene in the Cambridge sequential total energy package code.[35] The critical structure at threshold reaction pressure (12.2 GPa) of azulene was optimized with a space group $P2_1$ lattice (a = 6.61 Å, b = 5.49 Å, c = 7.09 Å, and β = 96.69°) based on the in situ XRD experiment. Generalized gradient approximation and the Perdew−Burke−Ernzerhof exchange−correlation functional were used.[36] The cutoff energy was set to 720 eV, and the k-point solution was better than 0.05 × 2π A^{-1}.

RESULTS AND DISCUSSION

Synthesis of CNTh and XRD Analysis. At ambient conditions, azulene crystallizes in a monoclinic lattice ($P2_1/c$, a = 9.94 Å, b = 5.98 Å, c = 7.88 Å, and β = 129.53°). The azulene molecules are parallelly stacked with some disordered antiphase orientations (Figure 1c).[37,38] We directly compressed azulene using a PE press to 20 GPa. After recovering to ambient conditions, we removed the unreacted azulene with ethanol, and ∼10 mg of an orange solid product (PE-20) was obtained. The different colors between PE-20 and azulene (blue) indicate a reaction. Since the blue color of azulene originates from the gap between the ground state (S_0) to the first excited state ($S_0 \rightarrow S_1$) and $S_0 \rightarrow S_2$,[39,40] the orange color of the product suggests a drastic irreversible change of electron energy levels, which is also verified by subsequent UV−vis absorption spectra. This observation aligns with numerous reports, indicating that changes in the structure of azulene lead to corresponding changes in absorption.[41−43]

The XRD data of PE-20 show a series of diffraction peaks at 7.7, 6.7, 4.8, and 3.9 Å. The peaks at 7.7 and 3.9 Å almost overlap with the 100 and 200 peaks of azulene, and the new 6.7 Å peak indicates the formation of a new structure. This "partially preserved" XRD pattern is a typical feature of high-pressure topochemical reactions (Figure 2a), indicating that polymerization extended along one dimension while the ordering along the a-axis remained almost unchanged. Such features of topochemical reaction are supported by many studies on 1,4-diphenylbutadiyne, azobenzene, s-triazine, and others.[44−46] For example, in the single-crystal polymerization of $C_{10}H_8 \cdot C_{10}F_8$,[21] the retention of single-crystal diffractions perpendicular to the direction of polymerization propagation reveals the preservation of long-range order, and the positions of the diffraction points in the XRD image show that the overall topology of the stacked monomers is preserved in the extended CNTs. Similarly, in the topochemical reaction of 2,5-furandicarboxylic acid,[15,16] the molecules polymerized along the c-direction, and the $hk0$ diffractions of the nanothread product almost coincide with the precursor, similar to the case of azulene. Additionally, the loss of high-angle Bragg peaks in the product also coincides with the formation of a nanothread structure as the nanothread often lacks precise atomic ordering, which is also a feature observed in disubstituted benzene CNTs.[47] Combining the above discussion, we can propose the 1-D polymerization of azulene.

Electron Diffraction and Microscopy. The CNTh structure was further demonstrated by SAED and HRTEM. As depicted in Figure 2b, the product exhibits a SAED pattern with pseudohexagonal symmetry, providing compelling evidence that nanothreads were formed with quasi-hexagonal packing. This is similar to those observed in benzene, aniline, s-triazine, phenol/pentafluorophenol cocrystals, and pyridine CNTs,[13,17,46,48,49] where a (pseudo-)6-fold diffraction pattern was observed. This pseudohexagonal $hk0$ diffraction feature results from the pseudohexagonal stacking of the threads. The interthread interactions are typically very weak and cannot maintain ordering along the thread direction, so hkl ($l \neq 0$) diffractions are absent. The observed diffractions with d = 7.8, 7.0, and 6.7 Å are indexed as 100, −110, and 010, accordingly,

https://doi.org/10.1021/acs.jpcc.4c04557
J. Phys. Chem. C 2024, 128, 16011−16019

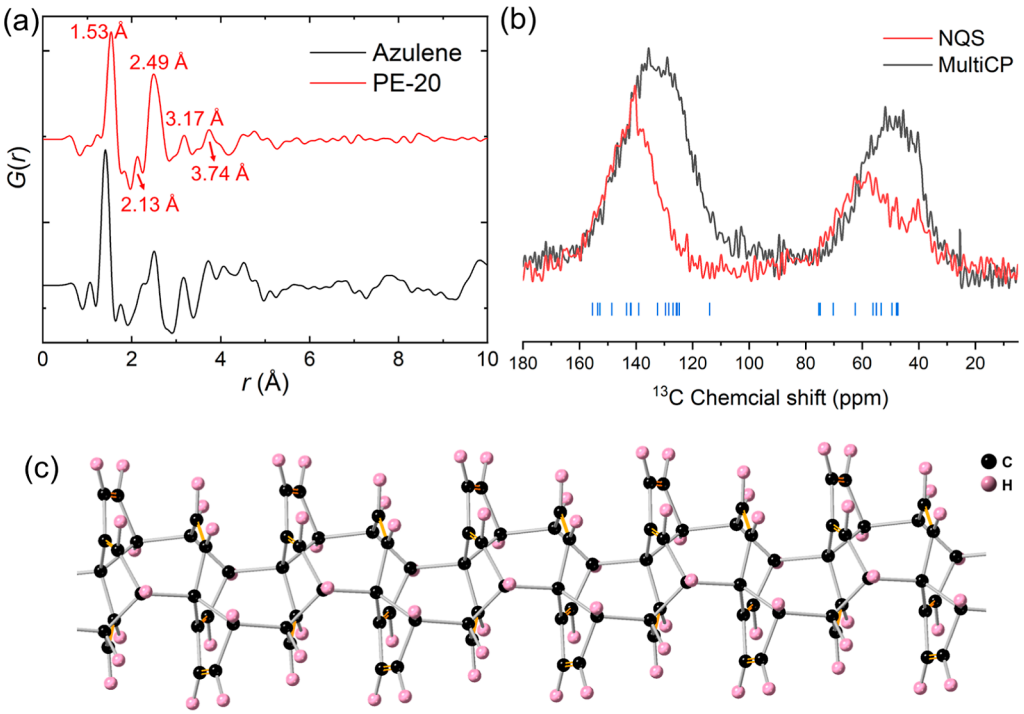

Figure 3. (a) PDF $G(r)$ plot of azulene and PE-20. (b) Quantitative multiCP and NQS ^{13}C ssNMR spectra. The vertical bars represent the simulated chemical shifts. (c) Proposed intrathread structure of azulene-CNTh.

corresponding to the projection along the thread direction. These *d*-values are consistent with the XRD results, suggesting that a peak at 7.0 Å presented in the XRD pattern, which was then identified by fitting of the overlapped peaks (Figure 2a). The SAED pattern also shows high-order diffractions, with the minimum *d*-spacing down to 3.3 Å (020). This contrasts with many previous studies of aromatic CNThs, like furan, phenol/pentafluorophenol cocrystal, and pyridine, which show only the first-order diffraction spots or rings at around d = 5−6 Å,[13,48,49] and suggests significantly improved crystallinity of azulene-CNTh. The good ordering should be attributed to the oriented stacking of the molecules, which highlights the intermolecular electrostatic interactions and the large nonrotational fused-ring skeleton. For the ordering along the thread (*c*-axis), no related diffraction was observed in XRD and SAED. This suggests that either the intrathread structure or the shift between the threads is disordered, making it impossible to quantify the *c*-axis. This phenomenon has been observed in numerous CNTh reports, such as those on benzene,[1] furan,[13] and pyridine nanothreads,[49] where the diffraction points of *hkl* ($l \neq 0$) cannot be observed.

The thread formation is further confirmed by the HRTEM image, which shows parallel striations (Figure 2c), indicating a 1D thread structure. These are similar to the polymerized products of benzene,[1] cubane,[50] and aniline.[17] The 7.4 Å spacing between the striations is consistent with the diffraction peak observed by the X-rays (d = 7.7 or 7.0 Å), considering that TEM typically has an uncertainty in the length scale of around 5%. We also observed the HRTEM pattern on the cross-section of the thread (Figure 2d), whose FFT image shows a pseudohexagonal pattern similar to the SAED pattern, confirming consistency between these observations. The difference in the *d*-spacing is attributed to the different orientations of the domains. Combining the XRD and SAED results, we conclude that the lattice of the product is a = 9.23 Å, b = 7.85 Å, and γ = 121.0°. The stacking of the CNThs was then proposed with the observed *hk*0 diffractions corresponding to the *d*-spacing of the interthread stacking shown in Figure 2e.

X-ray Total Scattering and NMR. To investigate the intrathread structure and reaction mechanism, we performed total X-ray scattering (Figures 3a and S2) and ssNMR measurements. As shown in the PDF $G(r)$ plot in Figure 3a, the peak assigned to the C−C bond length shifts from 1.41 Å in azulene to 1.53 Å in the product, highlighting a partial transition from sp^2-C to sp^3-C. The peak at 2.49 Å is therefore attributed to the C−C distance between the next closest neighboring sp^3 carbon atoms. Beyond ∼5 Å, the $G(r)$ plot shows a significant decay, primarily due to the lack of correlation between atoms from neighboring threads. This decay also suggests that the intrathread structure is short-range ordered on the atomic scale.

The local intrathread structure was further analyzed by using ssNMR. A quantitative ^{13}C NMR spectrum was measured using multiCP at 14 kHz MAS. It shows two bands at 49 and 130 ppm, corresponding to sp^3-C and sp^2-C, respectively (Figure 3b). The sp^3- and sp^2-C contents in the sample were obtained by peak integration of the MultiCP data using MestReNova software, with the former accounting for 38% of the total intensity (Figure S3). This suggests that, on average, four carbon atoms per azulene molecule are converted to sp^3-C. We also collected the nonquaternary suppression (NQS) NMR spectrum (Figure 3b), which only shows the peaks of carbons not bonded to H (C9 and C10). It displays two bands centered at 53 and 140 ppm, indicating the partial reaction of C9 and C10 in azulene. The peak shapes of the NQS and MultiCP spectra do not exactly overlap, which is attributed to the different chemical shifts of carbons not bonded to H atoms (C9 and C10) compared with those bonded to hydrogen atoms (C1−C8) in the same hybridization case. For example,

https://doi.org/10.1021/acs.jpcc.4c04557
J. Phys. Chem. C 2024, 128, 16011−16019

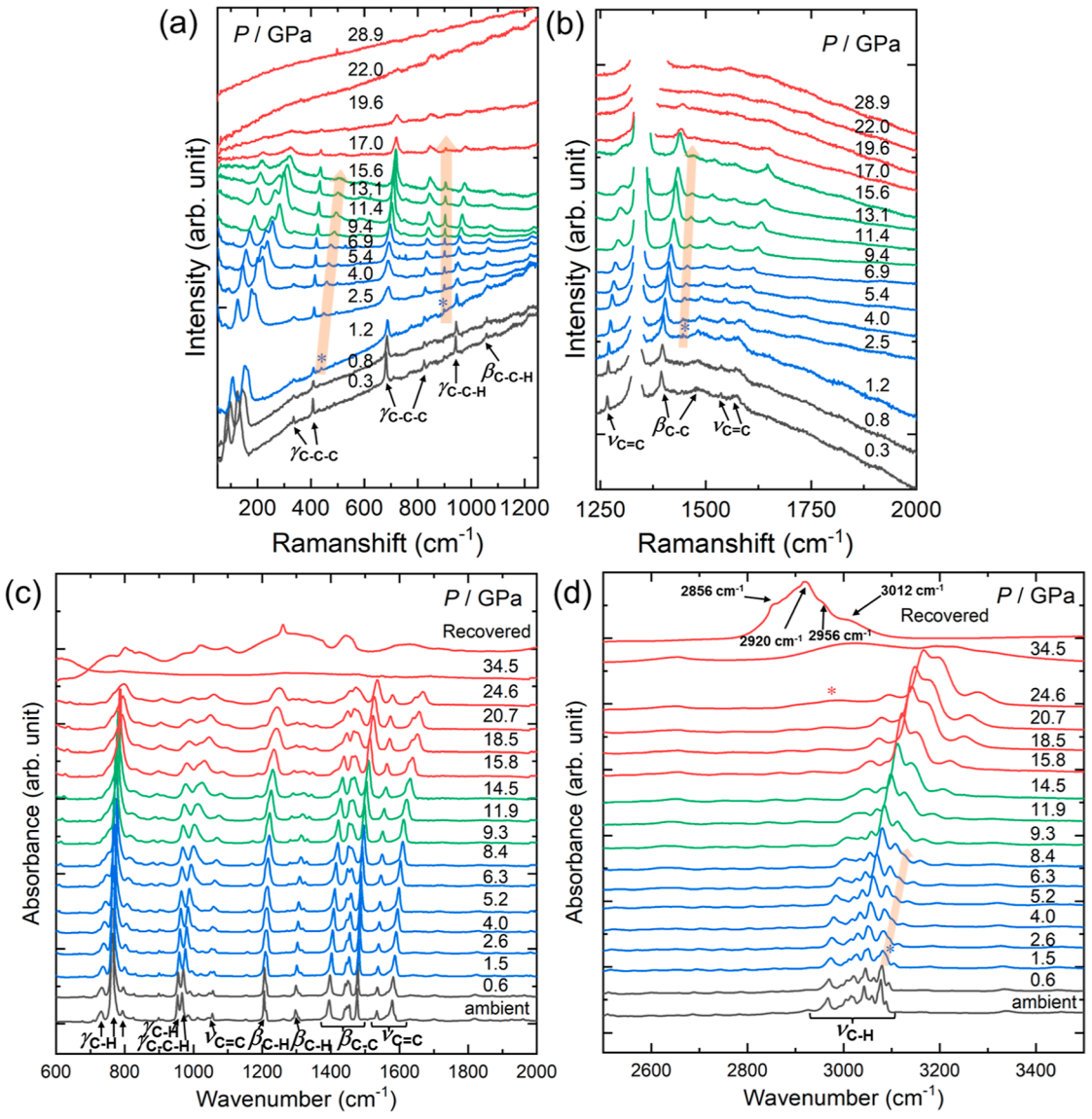

Figure 4. In situ Raman spectra of azulene upon compression in the spectral region of (a) 50−1250 cm^{-1} and (b) 1240−2000 cm^{-1}; in situ IR spectra upon compression in the spectral region of (c) 600−2000 cm^{-1} and (d) 2700−3400 cm^{-1}. The new peaks are marked by asterisks. The diamond Raman peaks from the DAC are removed for a better display.

the sp^2-C peak in NQS data shows a peak at 120−160 ppm, whereas the peak in MultiCP data has a wider distribution at 110−160 ppm. Thus, the portion at 110−120 ppm, probably extending to 140 ppm, is attributed to the sp^2-carbons bonded to hydrogen atoms (sp^2-C−H, originating from unreacted C1−C8) in the product. Similarly, the difference between MultiCP and NQS at 20−70 ppm stems from the sp^3-C−H. Therefore, these data also suggest that C1−C8 partially reacts in azulene.

Based on these results, we have a deeper understanding of the intrathread structure of the product: four carbon atoms in a molecule transform into sp^3-C on average, and both C9−C10 and C1−C8 partially transform into sp^3-C. Here, we propose one possible candidate CNTh model, where C3, C6, C7, and C10 are sp^3-hybridized, and the other atoms are sp^2-hybridized (Figure 3c). To compare the NMR shifts between the model and experiment, we constructed a model with a length of five molecular layers and simulated the NMR chemical shifts. As shown in Figure 3b, the simulated chemical shifts match the experimental results well. However, due to the disordered structure present in the samples, more experimental evidence is needed to determine the precise product structure.

In Situ Spectroscopy. To trace the polymerization process, we first performed in situ Raman experiments, and the detailed Raman peak assignments of azulene are listed in Table S1 according to a previous study.[51] As shown in Figure 4a,b, upon compression, the Raman peaks blue-shift slowly. At 1.2 GPa, the intensity of peaks at 439, 898, and 1446 cm^{-1} enhanced, which indicates a minor phase transition. Above 15.6 GPa, the intensity of most Raman peaks decreases and disappears at higher pressure, suggesting the onset reaction pressure of ∼15 GPa. After decompressing to ambient conditions (Figure S4), the sample only shows a strong photoluminescence signal, which evidences an irreversible process.

The irreversible reaction process was also observed in IR spectra (Figure 4c,d) and the assignments of IR peaks are presented in Table S1. As shown in Figure 4d, at 1.5 GPa, a shoulder peak emerged at 3090 cm^{-1} in the region of C−H

https://doi.org/10.1021/acs.jpcc.4c04557
J. Phys. Chem. C 2024, 128, 16011−16019

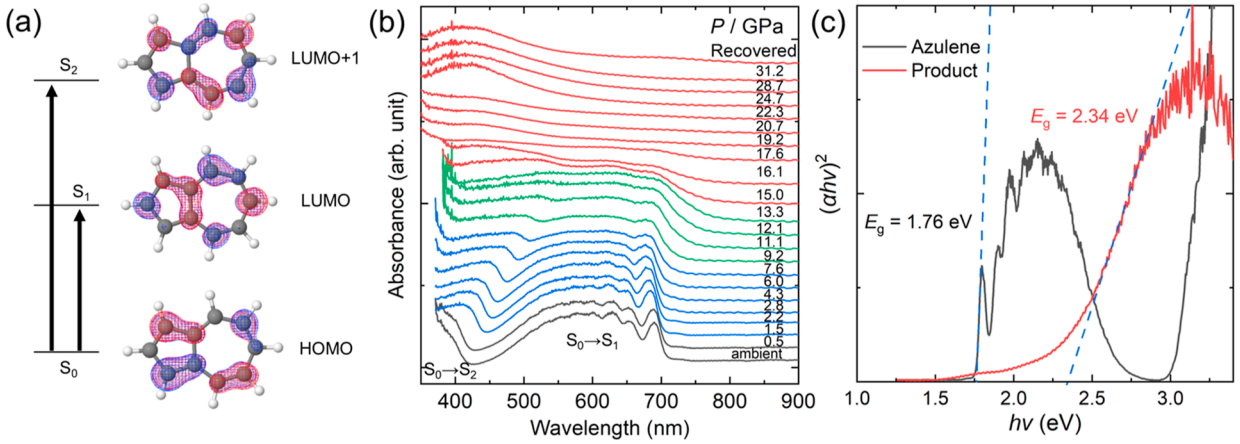

Figure 5. (a) Molecular orbitals of azulene, produced from the MolCalc website.[53] (b) In situ UV−vis spectra of azulene upon compression. (c) Tauc plot to determine the optical bandgap of azulene and the product, with extrapolation of the linear region estimating approximately 1.76 and 2.34 eV, respectively.

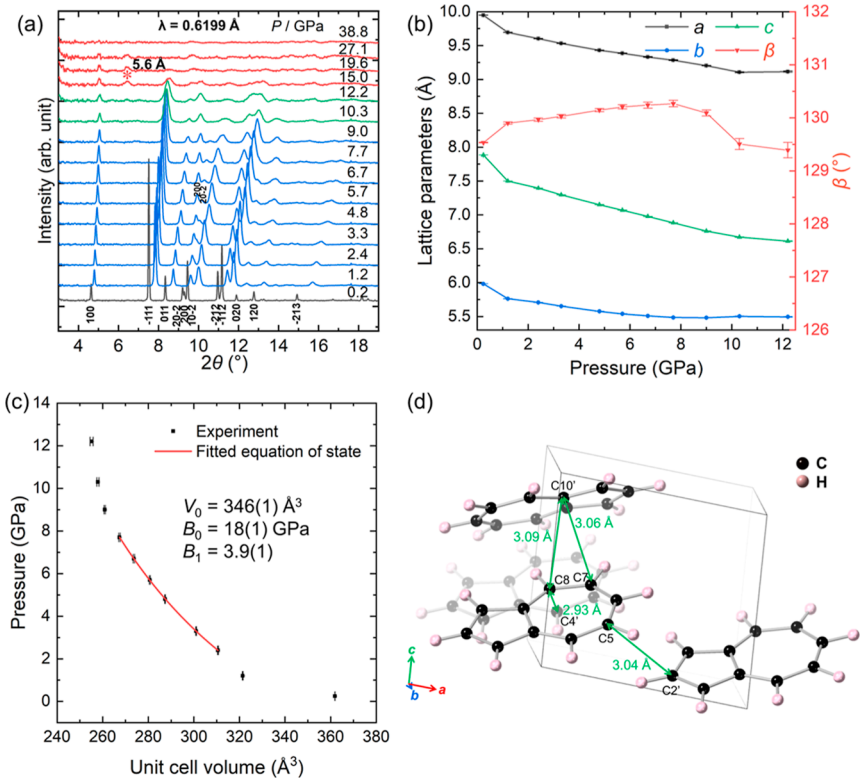

Figure 6. (a) In situ synchrotron XRD of azulene under high pressure. The evolution of (b) lattice parameters and (c) unit-cell volume of azulene with pressure, with error bars. (d) Crystal structure of azulene at 12.2 GPa.

stretching, consistent with the phase transition in the Raman spectra. Above 24.6 GPa, an obvious bulge emerged in the region of sp^3−C−H stretching (~2989 cm^{-1}), disclosing polymerization. After decompressing to ambient conditions, the IR spectrum of the product was consistent with that of PE-20, with sp^3 C−H vibration peaks at 2856, 2920, and 2956 cm^{-1}, demonstrating the irreversible polymerization and sp^3-CH presented in the product (Figure S5). The weak peak at 3012 cm^{-1} suggests that parts of the C1−C8 atoms are unreacted, resulting in residual sp^2-CH, as observed in ssNMR.

While azulene is blue, the product appears orange, indicating the change in absorption and electron energy level, as disclosed by in situ UV−vis absorption spectroscopy experiments. At ambient conditions, azulene exhibits a small energy gap between the ground state S_0 and the first excited state S_1, resulting from the nonmirror-related highest occupied molecular orbital and lowest unoccupied molecular orbital geometry that reduces the electronic repulsive interaction (Figure 5a).[39,40] Thus, $S_0 \rightarrow S_1$ and $S_0 \rightarrow S_2$ transitions of azulene show two absorption bands in the visible range and ultraviolet region, respectively, which endows it with a blue color. Upon compression, the $S_0 \rightarrow S_2$ absorption peak gradually red-shifts, while the $S_0 \rightarrow S_1$ absorption peak blue-shifts slowly (Figure 5b). It suggests that the $S_0 \rightarrow S_2$ gap decreased and the $S_0 \rightarrow S_1$ gap increased. Above 7.6 GPa, the $S_0 \rightarrow S_1$ absorption peak began to red-shift and overlapped

https://doi.org/10.1021/acs.jpcc.4c04557
J. Phys. Chem. C 2024, 128, 16011−16019

with the $S_0 \rightarrow S_2$ absorption peak. At 15 GPa, the intensity of the absorption peak of azulene started to decrease, which implies the onset of the reaction and is consistent with the Raman and IR experiments. At 24.7 GPa, a new absorption peak emerged at ∼400 nm and remained in the decompression process (Figure S6), which is attributed to $\pi \rightarrow \pi^*$ from sp^2-C. These sp^2-C defects also result in a product with an optical band gap of 2.34 eV (Figure 5c), which is much smaller than that of fully saturated benzene CNThs (>4.0 eV)[52] but larger than that of azulene (1.76 eV).

In Situ XRD under High Pressure. To investigate the structural evolution of azulene under high pressure, we collected in situ synchrotron XRD patterns up to 38.8 GPa. As shown in Figure 6a, from ambient pressure to 15 GPa, all the diffraction peaks shifted to a high angle, attributed to the compressed intermolecular distance. We then performed Rietveld refinements starting from the ambient-pressure structure (Figure S7 and Table S2−S4). The evolution of the lattice parameters was obtained up to 12.2 GPa and the $P-V$ relationship data shows a discontinuity at ∼1.2 GPa (Figure 6b), which evidences the phase transition observed in Raman and IR spectra. In addition, the curve shows a slight discontinuity at 9 GPa, which could be related to another minor phase transition or nonhydrostatic stress during compression and still needs to be investigated further. Thus, the $P-V$ relationship in the region of 2.7 to 7.7 GPa was then fitted using the third-order Birch−Murnaghan equation of state (Figure 6c)

$$P(V) = \frac{3}{2}B_0\left[\left(\frac{V_0}{V}\right)^{7/3} - \left(\frac{V_0}{V}\right)^{5/3}\right]\left\{1 + \frac{3}{4}(B_1 - 4)\left[\left(\frac{V_0}{V}\right)^{2/3} - 1\right]\right\}$$

where V_0 is the unit cell volume at ambient pressure, B_0 and B_1 are the isothermal bulk modulus and its first pressure derivative, with V_0 = 346(1) Å^3, B_0 = 18(1) GPa, and B_1 = 3.9(1). At 15.0 GPa, a new diffraction peak emerged at 6.4° (d = 5.6 Å) and the intensity of the −111 peak of azulene decreased obviously (Figure 6a), while the original 100 peak remained, which demonstrates the reaction of azulene and the generation of crystalline product. After being compressed to 38.8 GPa, all of the diffraction peaks are illegible.

To determine the critical structure of azulene, which refers to the crystal structure immediately preceding the reaction, we performed theoretical optimization combined with the cell parameters obtained from the Le Bail fitting of the 12.2 GPa data in XRD. In the calculations, to determine the exact intermolecular distances, we used an ordered $P2_1$ symmetry model.[37] As shown in Figure 6d, the azulene molecules exhibit a staggered stacking similar to the high-pressure phase of benzene rather than a columnar stacking. The nearest intermolecular C−C distances are determined with $d_{C5\cdots C2'}$ = 3.04 Å, $d_{C8\cdots C10'}$ = 3.09 Å, $d_{C7\cdots C10'}$ = 3.06 Å, and $d_{C8\cdots C4'}$ = 2.93 Å, which are close to the threshold distance of other aromatics.[54−56] Therefore, these closer pairs of carbon atoms may be the preferred sites for the reaction.

CONCLUSIONS

In summary, the structural evolution and reaction process of azulene upon compression were studied by in situ Raman, IR, and UV−vis spectra as well as XRD. Above 15 GPa, azulene experienced an irreversible reaction toward an orderly stacked CNTh product. The PDF and NMR measurements revealed that the product contains sp^2- and sp^3-C. The smallest d-spacing of the CNThs was down to 3.3 Å, in obvious contrast to many previous studies of the polyarene-CNThs. This should be attributed to the oriented stacking of the molecules, which is contributed by the intermolecular electrostatic interactions and the large nonrotational fused-ring skeleton. Our studies provide an important reference for understanding the reaction of aromatics under high pressure and benefit the design and synthesis of crystalline pure-carbon CNTh products. It also highlights a new reaction of azulene induced by high pressure and provides an alternative way to modify the electronic structure of azulene.

ASSOCIATED CONTENT

Supporting Information

The Supporting Information is available free of charge at https://pubs.acs.org/doi/10.1021/acs.jpcc.4c04557.

Lab XRD pattern with the Rietveld refinement plot of azulene at ambient conditions; HRTEM of PE-20 showing the linear structure of the product; integration plot of X-ray total scattering patterns and $S(q)$ plot of azulene and PE-20; in situ Raman spectra of azulene during decompression; IR spectra of azulene recovered from 34.5 GPa in a DAC and PE-20; UV−vis spectra of azulene upon decompression; Rietveld refinement results of the XRD pattern at 0.2 and 1.2 GPa; assignments of vibration modes of azulene; lattice parameters of azulene at 0.2 and 1.2 GPa; and atomic coordinates of azulene at 0.2 and 1.2 GPa (PDF)

AUTHOR INFORMATION

Corresponding Authors

Haiyan Zheng − *Center for High Pressure Science and Technology Advanced Research, Beijing 100193, P. R. China*; orcid.org/0000-0002-4727-5912; Email: zhenghy@hpstar.ac.cn

Kuo Li − *Center for High Pressure Science and Technology Advanced Research, Beijing 100193, P. R. China*; orcid.org/0000-0002-4859-6099; Email: likuo@hpstar.ac.cn

Authors

Xin Yang − *Center for High Pressure Science and Technology Advanced Research, Beijing 100193, P. R. China*

Guangwei Che − *Center for High Pressure Science and Technology Advanced Research, Beijing 100193, P. R. China*

Fang Li − *Center for High Pressure Science and Technology Advanced Research, Beijing 100193, P. R. China*

Xingyu Tang − *Center for High Pressure Science and Technology Advanced Research, Beijing 100193, P. R. China*

Yajie Wang − *Center for High Pressure Science and Technology Advanced Research, Beijing 100193, P. R. China*

Yida Wang − *Center for High Pressure Science and Technology Advanced Research, Beijing 100193, P. R. China*

Aijiao Guan − *Institute of Chemistry, Chinese Academy of Science, Beijing 100190, P. R. China*

Junfeng Xiang − *Institute of Chemistry, Chinese Academy of Science, Beijing 100190, P. R. China*

Qian Li − *Institute of Chemistry, Chinese Academy of Science, Beijing 100190, P. R. China;* orcid.org/0000-0003-3366-3858

Jie Liu − *Center for High Pressure Science and Technology Advanced Research, Beijing 100193, P. R. China*

Xiao Dong − *Key Laboratory of Weak-Light Nonlinear Photonics, School of Physics, Nankai University, Tianjin 300071, P. R. China;* orcid.org/0000-0003-4533-1914

Ho-kwang Mao − *Shanghai Key Laboratory MFree, Shanghai Advanced Research in Physical Sciences, Pudong, Shanghai 201203, P.R. China; Center for High Pressure Science and Technology Advanced Research, Beijing 100193, P. R. China*

Complete contact information is available at: https://pubs.acs.org/10.1021/acs.jpcc.4c04557

Notes

The authors declare no competing financial interest.

■ ACKNOWLEDGMENTS

The authors acknowledge the support of the National Natural Science Foundation of China (grant no.: 22022101). The authors also acknowledge the support of the National Key Research and Development Program of China (2019YFA0708502). H.-k. Mao acknowledges the financial support from Shanghai Key Laboratory of MFree, China (No. 22dz2260800) and Shanghai Science and Technology Committee, China (No. 22JC1410300). This work was carried out with the support of the 4W2 beamline at the Beijing Synchrotron Radiation Facility and the 15U1 beamline at the Shanghai Synchrotron Radiation Facility. The pair distribution function data were collected at the 11-ID-B beamline of the Advanced Photon Source at the Argonne National Laboratory and the 13HB beamline of the Shanghai Synchrotron Radiation Facility. This study was partially supported by the Synergic Extreme Condition User Facility (SECUF).

■ REFERENCES

(1) Fitzgibbons, T. C.; Guthrie, M.; Xu, E. S.; Crespi, V. H.; Davidowski, S. K.; Cody, G. D.; Alem, N.; Badding, J. V. Benzene-Derived Carbon Nanothreads. *Nat. Mater.* **2015**, *14*, 43−47.

(2) Roman, R. E.; Kwan, K.; Cranford, S. W. Mechanical Properties and Defect Sensitivity of Diamond Nanothreads. *Nano Lett.* **2015**, *15*, 1585−1590.

(3) Feng, C.; Xu, J.; Zhang, Z.; Wu, J. Morphology- and Dehydrogenation-Controlled Mechanical Properties in Diamond Nanothreads. *Carbon* **2017**, *124*, 9−22.

(4) Silveira, J. F. R. V.; Muniz, A. R. First-Principles Calculation of the Mechanical Properties of Diamond Nanothreads. *Carbon* **2017**, *113*, 260−265.

(5) Zhan, H.; Zhang, G.; Zhang, Y.; Tan, V. B. C.; Bell, J. M.; Gu, Y. Thermal Conductivity of a New Carbon Nanotube Analog: The Diamond Nanothread. *Carbon* **2016**, *98*, 232−237.

(6) Silveira, J. F.; Muniz, A. R. Functionalized Diamond Nanothreads from Benzene Derivatives. *Phys. Chem. Chem. Phys.* **2017**, *19*, 7132−7137.

(7) Zhu, T.; Ertekin, E. Phonons, Localization, and Thermal Conductivity of Diamond Nanothreads and Amorphous Graphene. *Nano Lett.* **2016**, *16*, 4763−4772.

(8) Zhan, H.; Zhang, G.; Bell, J. M.; Gu, Y. The Morphology and Temperature Dependent Tensile Properties of Diamond Nanothreads. *Carbon* **2016**, *107*, 304−309.

(9) Zhan, H.; Zhang, G.; Bell, J. M.; Tan, V. B. C.; Gu, Y. High Density Mechanical Energy Storage with Carbon Nanothread Bundle. *Nat. Commun.* **2020**, *11*, 1905.

(10) Chen, B.; Hoffmann, R.; Ashcroft, N. W.; Badding, J.; Xu, E.; Crespi, V. Linearly Polymerized Benzene Arrays as Intermediates, Tracing Pathways to Carbon Nanothreads. *J. Am. Chem. Soc.* **2015**, *137*, 14373−14386.

(11) Juhl, S. J.; Wang, T.; Vermilyea, B.; Li, X.; Crespi, V. H.; Badding, J. V.; Alem, N. Local Structure and Bonding of Carbon Nanothreads Probed by High-Resolution Transmission Electron Microscopy. *J. Am. Chem. Soc.* **2019**, *141*, 6937−6945.

(12) Duan, P.; Li, X.; Wang, T.; Chen, B.; Juhl, S. J.; Koeplinger, D.; Crespi, V. H.; Badding, J. V.; Schmidt-Rohr, K. The Chemical Structure of Carbon Nanothreads Analyzed by Advanced Solid-State NMR. *J. Am. Chem. Soc.* **2018**, *140*, 7658−7666.

(13) Huss, S.; Wu, S.; Chen, B.; Wang, T.; Gerthoffer, M. C.; Ryan, D. J.; Smith, S. E.; Crespi, V. H.; Badding, J. V.; Elacqua, E. Scalable Synthesis of Crystalline One-Dimensional Carbon Nanothreads through Modest-Pressure Polymerization of Furan. *ACS Nano* **2021**, *15*, 4134−4143.

(14) Matsuura, B. S.; Huss, S.; Zheng, Z.; Yuan, S.; Wang, T.; Chen, B.; Badding, J. V.; Trauner, D.; Elacqua, E.; van Duin, A. C. T.; et al. Perfect and Defective ^{13}C-Furan-Derived Nanothreads from Modest-Pressure Synthesis Analyzed by ^{13}C NMR. *J. Am. Chem. Soc.* **2021**, *143*, 9529−9542.

(15) Wang, X.; Yang, X.; Wang, Y.; Tang, X.; Zheng, H.; Zhang, P.; Gao, D.; Che, G.; Wang, Z.; Guan, A.; et al. From Biomass to Functional Crystalline Diamond Nanothread: Pressure-Induced Polymerization of 2,5-Furandicarboxylic Acid. *J. Am. Chem. Soc.* **2022**, *144*, 21837−21842.

(16) Dunning, S. G.; Chen, B.; Zhu, L.; Cody, G. D.; Chariton, S.; Prakapenka, V. B.; Zhang, D.; Strobel, T. A. Synthesis and Post-Processing of Chemically Homogeneous Nanothreads from 2,5-Furandicarboxylic Acid. *Angew. Chem., Int. Ed.* **2023**, *135*, No. e202217023.

(17) Nobrega, M. M.; Teixeira-Neto, E.; Cairns, A. B.; Temperini, M. L. A.; Bini, R. One-Dimensional Diamondoid Polyaniline-like Nanothreads from Compressed Crystal Aniline. *Chem. Sci.* **2018**, *9*, 254−260.

(18) Cockcroft, J. K.; Rosu-Finsen, A.; Fitch, A. N.; Williams, J. H. The temperature dependence of C−H-F−C interactions in benzene: hexafluorobenzene. *CrystEngComm* **2018**, *20*, 6677−6682.

(19) Coates, G. W.; Dunn, A. R.; Henling, L. M.; Dougherty, D. A.; Grubbs, R. H. Phenyl-Perfluorophenyl Stacking Interactions: a New Strategy for Supermolecule Construction. *Angew. Chem., Int. Ed.* **1997**, *36*, 248−251.

(20) Gdaniec, M.; Jankowski, W.; Milewska, M. J.; Połoński, T. Supramolecular Assemblies of Hydrogen-Bonded Carboxylic Acid Dimers Mediated by Phenyl-Pentafluorophenyl Stacking Interactions. *Angew. Chem., Int. Ed.* **2003**, *42*, 3903−3906.

(21) Ward, M. D.; Tang, W. S.; Zhu, L.; Popov, D.; Cody, G. D.; Strobel, T. A. Controlled Single-Crystalline Polymerization of $C_{10}H_8$·$C_{10}F_8$ under Pressure. *Macromolecules* **2019**, *52*, 7557−7563.

(22) Friedrich, A.; Collings, I. E.; Dziubek, K. F.; Fanetti, S.; Radacki, K.; Ruiz-Fuertes, J.; Pellicer-Porres, J.; Hanfland, M.; Sieh, D.; Bini, R.; et al. Pressure-Induced Polymerization of Polycyclic Arene-Perfluoroarene Cocrystals: Single Crystal X-ray Diffraction Studies, Reaction Kinetics, and Design of Columnar Hydrofluorocarbons. *J. Am. Chem. Soc.* **2020**, *142*, 18907−18923.

(23) Xin, H.; Hou, B.; Gao, X. Azulene-Based π-Functional Materials: Design, Synthesis, and Applications. *Acc. Chem. Res.* **2021**, *54*, 1737−1753.

(24) Xia, J.; Capozzi, B.; Wei, S.; Strange, M.; Batra, A.; Moreno, J. R.; Amir, R. J.; Amir, E.; Solomon, G. C.; Venkataraman, L.; et al. Breakdown of Interference Rules in Azulene, a Nonalternant Hydrocarbon. *Nano Lett.* **2014**, *14*, 2941−2945.

(25) Anderson, A. G.; Steckler, B. M.; Azulene, V. I. I. I. A Study of the Visible Absorption Spectra and Dipole Moments of some 1-and 1,3-Substituted Azulenes. *J. Am. Chem. Soc.* **1959**, *81*, 4941−4946.

(26) Piacenza, M.; Grimme, S. Van der Waals Complexes of Polar Aromatic Molecules: Unexpected Structures for Dimers of Azulene. *J. Am. Chem. Soc.* **2005**, *127*, 14841−14848.

(27) Salmon, P. S.; Drewitt, J. W. E.; Whittaker, D. A. J.; Zeidler, A.; Wezka, K.; Bull, C. L.; Tucker, M. G.; Wilding, M. C.; Guthrie, M.; Marrocchelli, D. Density-Driven Structural Transformations in Network Forming Glasses: a High-Pressure Neutron Diffraction Study of GeO_2 Glass up to 17.5 GPa. *J. Phys. Condens. Matter* **2012**, *24*, 415102.
(28) Mao, H. K.; Xu, J.; Bell, P. M. Calibration of the Ruby Pressure Gauge to 800 kbar under Quasi-Hydrostatic Conditions. *J. Geophys. Res.* **1986**, *91*, 4673−4676.
(29) Prescher, C.; Prakapenka, V. B. DIOPTAS: a Program for Reduction of Two-Dimensional X-Ray Diffraction Data and Data Exploration. *High Pressure Res.* **2015**, *35*, 223−230.
(30) Petříček, V.; Dušek, M.; Palatinus, L. Crystallographic Computing System JANA2006: General features. *Z. Kristallogr. Cryst. Mater.* **2014**, *229*, 345−352.
(31) Johnson, R. L.; Schmidt-Rohr, K. Quantitative solid-state ^{13}C NMR with signal enhancement by multiple cross polarization. *J. Magn. Reson.* **2014**, *239*, 44−49.
(32) Lodewyk, M. W.; Siebert, M. R.; Tantillo, D. J. Computational prediction of ^{1}H and ^{13}C chemical shifts: a useful tool for natural product, mechanistic, and synthetic organic chemistry. *Chem. Rev.* **2012**, *112*, 1839−1862.
(33) Jain, R.; Bally, T.; Rablen, P. R. Calculating accurate proton chemical shifts of organic molecules with density functional methods and modest basis sets. *J. Org. Chem.* **2009**, *74*, 4017−4023.
(34) Juhás, P.; Davis, T.; Farrow, C. L.; Billinge, S. J. L. PDFgetX3: a Rapid and Highly Automatable Program for Processing Powder Diffraction Data into Total Scattering Pair Distribution Functions. *J. Appl. Crystallogr.* **2013**, *46*, 560−566.
(35) Clark, S. J.; Segall, M. D.; Pickard, C. J.; Hasnip, P. J.; Probert, M. I. J.; Refson, K.; Payne, M. C. First Principles Methods Using CASTEP. *Z. Kristallogr.* **2005**, *220*, 567−570.
(36) Perdew, J. P.; Burke, K.; Ernzerhof, M. Generalized Gradient Approximation Made Simple. *Phys. Rev. Lett.* **1996**, *77*, 3865−3868.
(37) Dittrich, B.; Fabbiani, F. P. A.; Henn, J.; Schmidt, M. U.; Macchi, P.; Meindl, K.; Spackman, M. A. Azulene Revisited: Solid-State Structure, Invariom Modeling and Lattice-Energy Minimization of a Classical Example of Disorder. *Acta Crystallogr.* **2018**, *74*, 416−426.
(38) Bräuniger, T.; Poupko, R.; Luz, Z.; Gutsche, P.; Meinel, C.; Zimmermann, H.; Haeberlen, U. The Dynamic Disorder of Azulene: A Single Crystal Deuterium Nuclear Magnetic Resonance Study. *J. Chem. Phys.* **2000**, *112*, 10858−10870.
(39) Liu, R. S. H. Colorful Azulene and Its Equally Colorful Derivatives. *J. Chem. Educ.* **2002**, *79*, 183−185.
(40) Dunlop, D.; Ludvíková, L.; Banerjee, A.; Ottosson, H.; Slanina, T. Excited-State (Anti)Aromaticity Explains Why Azulene Disobeys Kasha's Rule. *J. Am. Chem. Soc.* **2023**, *145*, 21569−21575.
(41) Liu, R. S. H.; Muthyala, R. S.; Wang, X.-s.; Asato, A. E.; Wang, P.; Ye, C. Correlation of Substituent Effects and Energy Levels of the Two Lowest Excited States of the Azulenic Chromophore. *Org. Lett.* **2000**, *2*, 269−271.
(42) Tsuchiya, T.; Hamano, T.; Inoue, M.; Nakamura, T.; Wakamiya, A.; Mazaki, Y. Intense Absorption of Azulene Realized by Molecular Orbital Inversion. *Chem. Commun.* **2023**, *59*, 10604−10607.
(43) Chamelot, G.; Idir, M.; Leclerc, M.; Morin, J.-F. Synthesis and Properties of 2,6-Azulene-Based Conjugated Polymers and Their Applications in Dispersing Single-Walled Carbon Nanotubes. *Polym. Chem.* **2023**, *14*, 1206−1212.
(44) Zhang, P.; Tang, X.; Wang, Y.; Wang, X.; Gao, D.; Li, Y.; Zheng, H.; Wang, Y.; Wang, X.; Fu, R.; et al. Distance-Selected Topochemical Dehydro-Diels-Alder Reaction of 1,4-Diphenylbutadiyne toward Crystalline Graphitic Nanoribbons. *J. Am. Chem. Soc.* **2020**, *142*, 17662−17669.
(45) Zhang, P.; Gao, D.; Tang, X.; Yang, X.; Zheng, H.; Wang, Y.; Wang, X.; Xu, J.; Wang, Z.; Liu, J.; et al. Ordered Van der Waals Hetero-nanoribbon from Pressure-Induced Topochemical Polymerization of Azobenzene. *J. Am. Chem. Soc.* **2023**, *145*, 6845−6852.
(46) Gao, D.; Tang, X.; Xu, J.; Yang, X.; Zhang, P.; Che, G.; Wang, Y.; Chen, Y.; Gao, X.; Dong, X.; et al. Crystalline $C_3N_3H_3$ Tube (3,0) Nanothreads. *Proc. Natl. Acad. Sci. U.S.A.* **2022**, *119*, No. e2201165119.
(47) Tang, W. S.; Strobel, T. A. Evidence for Functionalized Carbon Nanothreads from π-Stacked, para-Disubstituted Benzenes. *J. Phys. Chem. C* **2020**, *124*, 25062−25070.
(48) Gerthoffer, M. C.; Wu, S.; Chen, B.; Wang, T.; Huss, S.; Oburn, S. M.; Crespi, V. H.; Badding, J. V.; Elacqua, E. Sacrificial' Supramolecular Assembly and Pressure-Induced Polymerization: toward Sequence-Defined Functionalized Nanothreads. *Chem. Sci.* **2020**, *11*, 11419−11424.
(49) Li, X.; Wang, T.; Duan, P.; Baldini, M.; Huang, H. T.; Chen, B.; Juhl, S. J.; Koeplinger, D.; Crespi, V. H.; Schmidt-Rohr, K.; et al. Carbon Nitride Nanothread Crystals Derived from Pyridine. *J. Am. Chem. Soc.* **2018**, *140*, 4969−4972.
(50) Huang, H.; Zhu, L.; Ward, M. D.; Wang, T.; Chen, B.; Chaloux, B. L.; Wang, Q.; Biswas, A.; Gray, J. L.; Kuei, B.; et al. Nanoarchitecture through Strained Molecules: Cubane-Derived Scaffolds and the Smallest Carbon Nanothreads. *J. Am. Chem. Soc.* **2020**, *142*, 17944−17955.
(51) Chao, R. S.; Khanna, R. K. Resonace Raman Spectra and Vibrational Assignments of Azulene-d_0 and Azulene-d_8. *Spectrochim. Acta* **1975**, *33A*, 53−62.
(52) Demingos, P. G.; Muniz, A. R. Electronic and Mechanical Properties of Partially Saturated Carbon and Carbon Nitride Nanothreads. *J. Phys. Chem. C* **2019**, *123*, 3886−3891.
(53) Jensen, J. H.; Kromann, J. C. The Molecule Calculator: A Web Application for Fast Quantum Mechanics-Based Estimation of Molecular Properties. *J. Chem. Educ.* **2013**, *90*, 1093−1095.
(54) Wang, Y.; Dong, X.; Tang, X.; Zheng, H.; Li, K.; Lin, X.; Fang, L.; Sun, G.; Chen, X.; Xie, L.; et al. Pressure-Induced Diels-Alder Reactions in C_6H_6-C_6F_6 Cocrystal towards Graphane Structure. *Angew. Chem., Int. Ed.* **2019**, *58*, 1468−1473.
(55) Ciabini, L.; Santoro, M.; Gorelli, F. A.; Bini, R.; Schettino, V.; Raugei, S. Triggering Dynamics of the High-Pressure Benzene Amorphization. *Nat. Mater.* **2007**, *6*, 39−43.
(56) Tang, X.; Dong, X.; Zhang, C.; Li, K.; Zheng, H.; Mao, H.-k. Triggering Dynamics of Acetylene Topochemical Polymerization. *Matter Radiat. Extr.* **2023**, *8*, 058402.

https://doi.org/10.1021/acs.jpcc.4c04557
J. Phys. Chem. C 2024, 128, 16011−16019